

Ultra-High Toughness Fibers Using Controlled Disorder of Assembled Aramid Nanofibers

Hyun Chan Kim and Henry Angelo Sodano*

Assembling nanoscale building blocks with reduced defects has emerged as a promising approach to exploit nanomaterials in the fabrication of simultaneously strong and tough architectures at larger scales. Aramid nanofibers (ANFs), a type of organic nanobuilding block, have been spotlighted due to their superior mechanical properties and thermal stability. However, no breakthrough research has been conducted on the high mechanical properties of a structure composed of ANFs. Here, assembling ANFs into macroscale fiber using a simultaneous protonation and wet-spinning process is studied to reduce defects and control disorder. The ANF-assembled fibers consist of hierarchically aligned nanofibers that behave as a defective law structure, making it possible to reach a Young's modulus of 53.15 ± 8.98 GPa, a tensile strength of $1,353.64 \pm 92.98$ MPa, and toughness of 128.66 ± 14.13 MJ m⁻³. Compared to commercial aramid fibers, the fibers exhibit ≈ 1.6 times greater toughness while also providing specific energy to break as 93 J g⁻¹. Furthermore, this shows recyclability of the ANF assembly by retaining $\approx 94\%$ of the initial mechanical properties. This study demonstrates a facile process to produce high stiffness and strength fibers composed of ANFs that possess significantly greater toughness than commercial synthetic fibers.

The reduced defect density observed at a nanoscale allows nanomaterials to exhibit exceptional physical, chemical, mechanical, electrical, and thermal properties.^[1–3] When structural materials are confined to the nanoscale, the low probability of defects yields superior strength, stiffness, and toughness. However, in structural applications, nanomaterials have been primarily restricted to nanofillers and additives that allow for tailoring the mechanical performance in nanocomposites and hybrid structures. Recently, the re-assembly of nanoscale building blocks into well-ordered macroscale architectures has emerged as a promising approach to exploit nanomaterials in the fabrication of structures that are simultaneously strong and tough. Therefore, to translate the exceptional properties of nanomaterials to a macroscale structure, it is critical to develop manufacturing strategies that allow for the precise and defect-free bridging of the nanoscale geometry.


1. Introduction

Nanomaterials have emerged as integral components in the design of macroscale materials with unprecedented functionalities for structural, electrical, and medical applications.

H. C. Kim, H. A. Sodano
Department of Aerospace Engineering
University of Michigan
Ann Arbor, MI 48109, USA
E-mail: hsodano@umich.edu

H. A. Sodano
Department of Materials Science and Engineering
University of Michigan
Ann Arbor, MI 48109, USA

H. A. Sodano
Department of Macromolecular Science and Engineering
University of Michigan
Ann Arbor, MI 48109, USA

 The ORCID identification number(s) for the author(s) of this article can be found under <https://doi.org/10.1002/adfm.202208661>.

© 2022 The Authors. Advanced Functional Materials published by Wiley-VCH GmbH. This is an open access article under the terms of the Creative Commons Attribution-NonCommercial-NoDerivs License, which permits use and distribution in any medium, provided the original work is properly cited, the use is non-commercial and no modifications or adaptations are made.

DOI: 10.1002/adfm.202208661

While some assembly techniques and methods to attain defect-free hierarchical ordering have been developed to convert nanoscale building blocks into macro and micro-scale synthetic materials,^[4–6] they typically utilize self-organizing properties into higher-order structures by relying on chemical interactions, entropy, electromagnetic field, fluid flows or evaporation-based planar confinement.^[7–9] One of the promising and emerging strategies that have merited considerable research interest is combining colloidal self-assembly with extrusion-based methods such as wet spinning.^[10–12] This manufacturing approach allows for the organization of colloidal building blocks into macroscale structures in a convenient, versatile, and controllable manner. Nonetheless, the self-organization of nanomaterials into macroscopic structures remains challenging due to the highly multidisciplinary nature of self-assembly processes, which require balancing chemistry and manufacturing parameters to produce complex macroscale structures with excellent mechanical properties.

Aramid nanofibers (ANFs) are a type of organic nanoscale building block that can be obtained as colloidal suspensions through the disassembly of macroscale aramid fibers (Kevlar) using a dissolution and deprotonation process.^[13] Kevlar has a significant waste stream, coming primarily from ballistic armor, which provides an opportunity to recycle and up-scale the waste materials into high-value products. For example, ANFs have been used as nanofillers in polymer nanocomposites,^[14]

interfacial and interlaminar reinforcement in fiber-reinforced composites,^[15,16] and assembled to form membranes and bucky papers for a wide range of applications.^[17,18] ANFs also display self-assembly behavior that makes them compatible with reprocessing via protonation, where hydrogen bonding interactions can be reintroduced to strengthen the material by protonating NH groups among the deprotonated ANFs for isolation. However, current approaches to assembling ANFs yield structures whose mechanical properties are considerably inferior to their precursor's aramid structure. For example, Wang et al. reported wet spun fibers made of pure ANFs with a Young's modulus of 14.0 GPa and a breaking strength of 416 MPa,^[19] and Liu et al. reported fibers made of neat ANFs with a tensile strength of 350 MPa whereas a neat aramid fiber has a strength of 3.6 GPa and modulus of 112 GPa.^[20] Although numerous studies based on ANFs have sought to emulate the high performance of commercial aramid fibers, to the best of our knowledge, no detailed study has been conducted on the principle or methodology to fabricate macroscale structures consisting of ANFs that attain exceptional mechanical properties. This study demonstrates new processing methodologies to assemble ANFs into macroscale fibers with hierarchical alignment and controlled disorder using a scalable wet-spinning process. The ANF-assembled fibers exhibit excellent mechanical properties comparable to synthetic and natural fibers such as spider silk, nanocellulose, nylon, and carbon nanotube fibers.^[9,21–24] By realizing a bottom-up re-organization of the ANF network into macroscale fibers, it becomes possible to reimagine the process of fabricating high-performance macroscale crystalline solids that emulate and exceed the mechanical properties of hierarchical biological materials for a wide range of structural applications. This work further demonstrates the recyclability of the prepared ANF-assembled fibers to cope with the present environmental issues, which suggests their potential to be novel sustainable fibers that can be repeatedly reprocessed with remarkable mechanical properties.

2. Results and Discussion

2.1. ANFs Isolation and Assembly

Nanoscale ANFs were obtained as a colloidal suspension in the DMSO-based system with several concentrations by varying the initial weight of the Kevlar added to the deprotonation and dissolution solution. The ANF colloidal suspensions have a homogeneous red color and darken as the concentration increases (Figure S1, Supporting Information). The morphology of the ANFs can be observed through AFM imaging which shows the processing approach yields well-dispersed fibers with diameters ranging from 4 to 12 nm and lengths of several micrometers (Figure S2, Supporting Information). The colloidal ANFs are assembled to form hierarchical macroscale fibers through a sequential wet spinning, stretching, and drying processes (Figure 1a). First, the as-prepared ANF colloidal suspensions were wet spun into a coagulant solution designed to provide a controlled rate of protonation using a high-precision fluid dispenser feeding a flat-tipped stainless-steel needle. Intermolecular bonds, including hydrogen bonds, are formed by

protonation of the ANFs through proton donors (water and HCl) in the coagulation bath resulting in the continuous formation of gel-state fibers. In this study, three different coagulation baths are evaluated to elucidate the effect of the protonation environment on the assembled macroscale ANF structure, namely: DI water to obtain a moderate protonation rate, a dilute aqueous HCl solution to obtain rapid protonation, and a dilute acetone solution to create reduced protonation rate due to the relatively lower density of proton donors (Figure 1b). The rate of protonation is an essential factor in the determination of the degree of disorder. When the ANF colloidal suspension passes through the needle, the ANFs aligned along the needle due to shear flow momentarily lose their alignment due to the die swell effect as they exit the needle.^[25,26] As the flow persists in this situation, the collapsed arrangement of ANFs is partially recovered by the shear stress between the fluid and the gravitational drawing force. In this wet spinning process, the ANFs are gradually assembled within the flow with the rate of assembly controlled by the protonation rate. In other words, spinning into the HCl solution shows a fast protonation, which leads to the assembly of the ANFs in the early stages of the flow, where many disordered ANFs exist. On the other hand, when spun into a dilute acetone solution, the fiber is formed relatively late in the flow due to the slow protonation rate, resulting in more aligned ANFs.

Following protonation, the gel-state ANF-assembled fibers are washed with DI water to remove residual KOH and DMSO, and then drawn along their length to enhance the ANFs' hierarchical orientation and reduce pores generated among the entangled ANFs due to rapid precipitation as solvent exchange occurs between the solvent and non-solvent. In previous studies, voids caused by the protonation of ANFs were left, resulting in aerogels.^[27] Thin ANF shell structures were also attempted through a coating process to reduce the voids, but low mechanical properties were reported.^[19] In this study, the voids are removed by the drawing process applied to the gel fibers obtained by wet spinning into the coagulation solution. To further improve the fiber density, drying was carried out while maintaining the tension from the drawing process, thereby generating a final intermolecular bond among the hierarchically aligned ANFs and finishing the assembly process. The structure obtained through this process is shown in the cross-sectional SEM images of Figure 1c and can be seen to be non-porous and with ANFs well-aligned in the fiber axis. Furthermore, the hierarchical alignment of the ANFs can be seen in surface SEM images (Figure 1e). The rough surface of the fibers can potentially work advantageously to form stable interfaces if embedded in a polymer matrix. EDS analysis confirms no residual salts or other reactants remain in the fiber after washing (Figure S3, Supporting Information). In addition, the toughness of the fiber can be shown through the formation of a knot with a small radius of curvature without the occurrence of any rupture or brittle failure (Figure 1d). The abrasion resistance of the fiber can be seen by the absence of failure in a long fiber loop pulled through a tight overhand knot.^[28]

A subsequent annealing process was investigated to improve the strength and stiffness of the prepared fibers. The use of heat treatment with a specific temperature and time has been suggested in order to alter the mechanical properties of

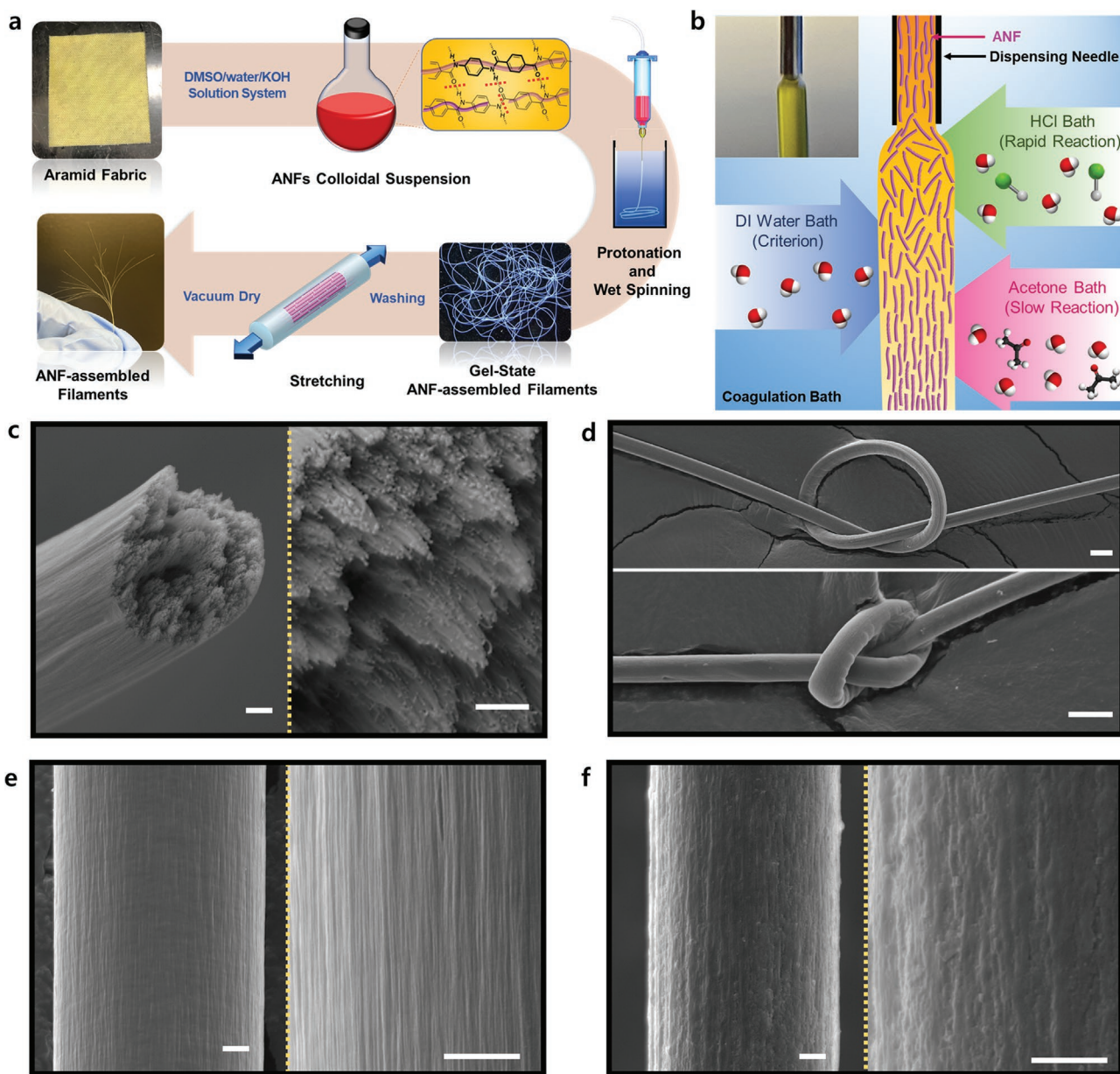


Figure 1. Assembly of ANFs to macroscale fibers. a) Flowchart of the fabrication process for ANF-assembled fibers. b) Illustration of ANFs assembly mechanism related to the relationship between the orientation of ANFs and protonation rate difference according to coagulation baths. c) SEM images of the cross-section of the fiber, showing the hierarchically aligned nanofibers. d) SEM images of the fiber knots. (e) SEM images of the surface of the fibers fabricated by a dilute acetone bath. f) SEM images of the surface of the fibers prepared through an additional annealing process. Scale bars in (c), (e), and (f) are 1 μm and (d) are 10 μm .

polymer materials through further densification, reduction of internal stress, and providing the energy required for chemical reactions.^[29] The annealing process of this study used a custom autoclave to simultaneously apply heat and pressure to fibers, thereby densifying the microstructure, which was verified through SEM imaging (Figure 1f).

The assembly of ANFs into a macroscale fiber is achieved here without the use of binders or cross-linkers, which is a fundamental bottom-up approach for assembly rather than forming a new type of ANF derivative or new molecular structures among the ANFs. The preservation of the molecular

structure can be shown through FTIR and XRD analysis. The FTIR spectra of ANF-assembled fibers and aramid fiber show identical absorption peaks indicating that no change in chemical structure occurs during the dissolution, gel spinning, and drawing processes (Figure 2a). XRD analysis shows no change in peak locations between each experimental condition, although the sharpness of peaks in the XRD patterns of ANF assembly is slightly diminished due to the decrease in the crystalline region, along with the reduced molecular density compared to the aramid fibers (Figure 2c). This hypothesis can be validated by analyzing the crystallinity, where the commercial

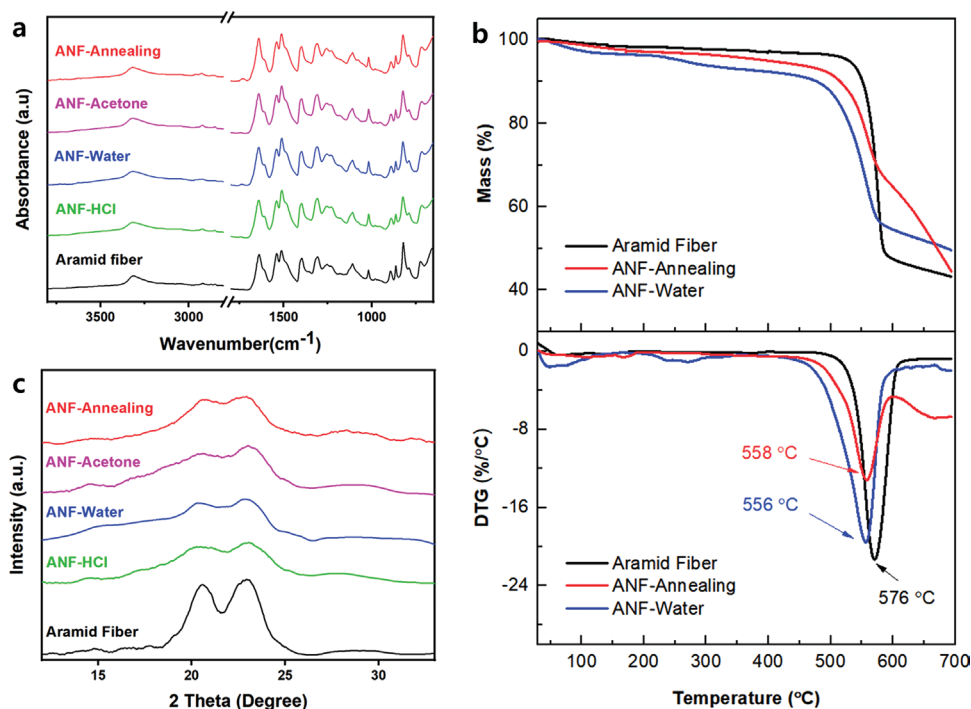


Figure 2. Chemical and thermal characteristics of commercial aramid fiber and ANF-assembled fibers. a) FTIR spectra, b) TGA and DTG curves, and c) XRD patterns.

aramid fibers have a crystallinity of 73% and the ANF-assembled fibers prepared with dilute acetone, DI water, and HCl solution have 53, 49, and 47% crystallinity, respectively. Furthermore, the fiber prepared through the annealing process showed increased crystallinity to 68%.

The thermal characteristics were analyzed for three different cases: commercial aramid fiber, ANF-assembled fiber within DI water, and annealed ANF-assembled fiber to confirm the effect of annealing. The decomposition temperature of the ANF-assembled fiber is 556 °C and increased to 558 °C through annealing, which are slightly lower values than the 576 °C decomposition temperature of the aramid fiber (Figure 2b). Aramid fibers are well known to possess a combination of high strength and thermal stability, and this result confirms that the ANF-assembled fibers retain the thermal stability of the precursor.

2.2. Mechanical Properties of ANF-Assembled Fibers

The relationship between the protonation rate and the degree of ANF alignment as a function of the assembly mechanism has been elucidated by evaluating the mechanical properties of the spun fibers. The maximum strength and modulus of the three different protonation environments are obtained using a dilute acetone bath with a 0.2 wt.% concentration of ANFs (Figure 3a). The dilute acetone solution provides a slow protonation rate, resulting in fibers with a high Young's modulus of 43.03 ± 2.72 GPa and tensile strength of 1353.64 ± 92.98 MPa. For comparison, fibers spun in a water bath show a modulus of 38.16 ± 3.75 GPa and tensile strength of 1234.40 ± 60.69 MPa,

while fibers spun in an HCl solution that provides rapid protonation has a modulus of 37.88 ± 3.33 GPa and tensile strength of 1166.51 ± 92.01 MPa. These results indicate that a slower protonation rate increases modulus and strength, but under an excessively slow protonation rate, the formation of a stable continuous gel fiber is hindered, causing the failure of the process (Figure S4, Supporting Information). The measured mechanical properties also correlate to the degree of alignment of ANFs, which is verified through azimuthal angle scanning by XRD (Figure 3e). The calculated orientation index f for the fiber is 0.44 in dilute acetone, 0.38 in water, and 0.37 in HCl solution, which means the fibers fabricated in dilute acetone are composed of the most significant number of well-aligned ANFs among the three conditions.

Tensile tests were performed to study the effect of ANF concentration in the colloidal suspension on the mechanical properties with fibers fabricated under four different concentrations (0.2%, 0.5%, 1.0%, and 1.5%) while the coagulation bath was fixed as dilute acetone (Figure 3b). The fibers made of 0.2 wt.% ANFs colloidal suspension show the greatest mechanical properties in this study, while the Young's modulus and tensile strength decrease as the concentration increases. This result occurs due to the die swelling effect which is amplified due to the increased viscosity as the ANF concentration in the colloidal solution is increased.^[26,30] The die swelling effect occurs at the exit of the dispensing needle and is the primary cause of disorder of the ANFs during the protonation process, which is demonstrated by the analysis of the X-ray azimuthal scanning on the prepared fibers with different concentrations (Figure S5, Supporting Information). On the other hand, increasing the concentration of solids increases the diameter

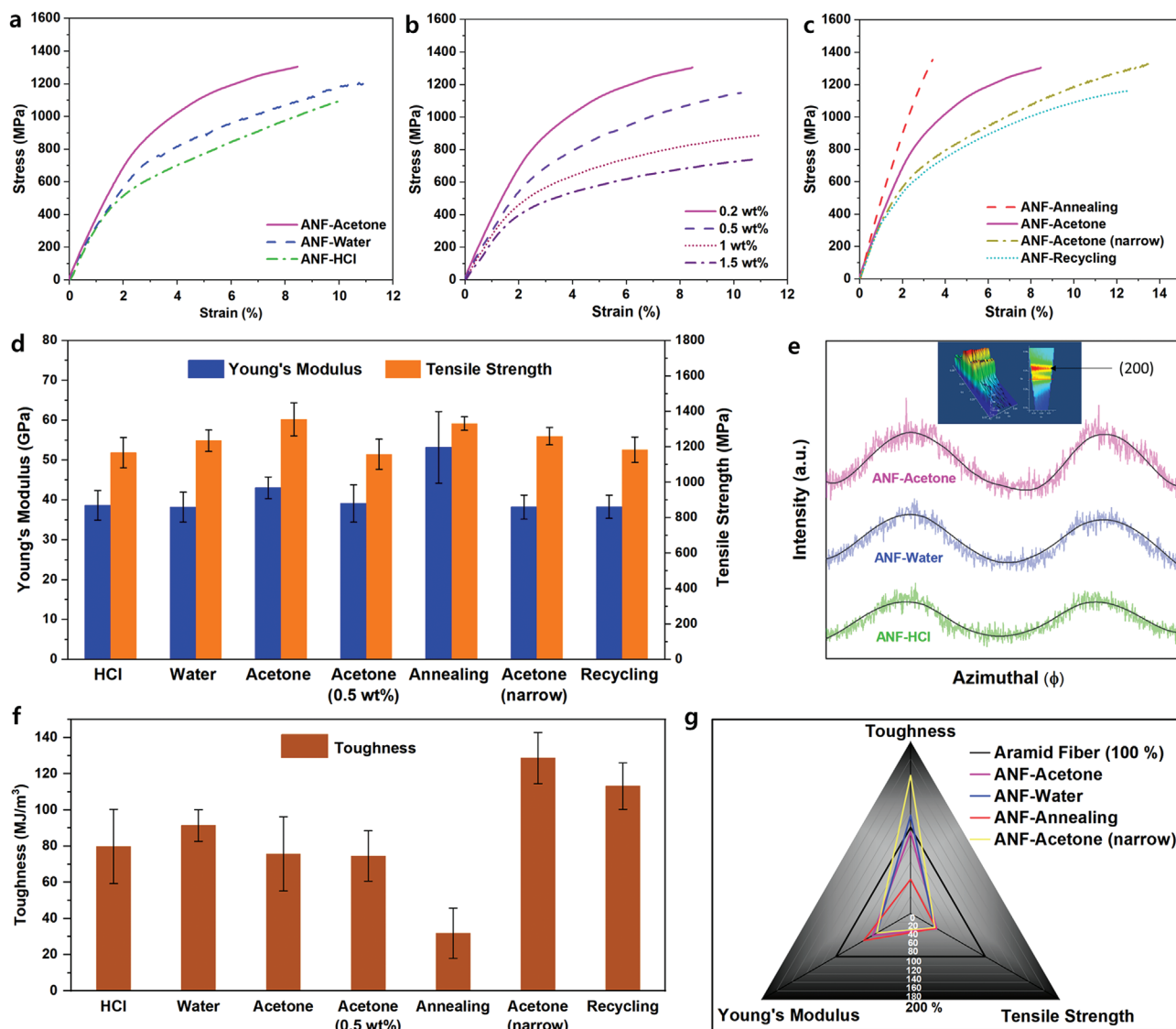


Figure 3. Mechanical characteristics of ANF-assembled fibers prepared in different conditions. Stress-strain curves to confirm the effect of a) coagulant baths indicating protonation rate influence, b) concentration of ANFs colloidal suspension, and c) additional annealing process, narrowed inner diameter of dispensing needle and recycling process on ANFs assembly and their mechanical properties. d) Comparison of the Young's modulus and tensile strength of the prepared fibers. e) Azimuthal intensity profiles at (200) plane of the fibers from different coagulant baths. f) Comparison of the toughness of the fibers. g) Radar chart for comparing the relative amount of three mechanical properties of the fibers based on commercial aramid fibers as reference (100%)

of the fiber (Table S1, Supporting Information), which leads to a decrease in strength because it can increase the density of defects.

Tensile testing was also conducted following post-spinning heat treatment to study the effect of annealing on the mechanical properties of the fibers. The mechanical properties of annealed fibers displayed a Young's modulus of 53.15 ± 8.98 GPa and tensile strength of 1330.20 ± 38.00 MPa. The elevated modulus is reported as the highest value in this study (Figure 3c,d). This result eventually proves that intermolecular bonding has been enriched due to heat and compression among aligned ANFs, which correlates to the increased crystallinity, thermal decomposition temperature, and structure density by the annealing step (Figures 1f,2b,c).

The exceptional toughness of Aramid fibers is well known, and therefore, fibers composed of ANFs should exhibit similarly high toughness. The toughness of each fiber was measured from the area under the tensile stress-strain curve. The results show a trade-off between toughness and modulus according to changes in ANFs orientation or by additional annealing steps except for the result from the dilute HCL when spinning parameters such as spinning speed and dispensing needle size are controlled (Figure 3d,f). The ANF alignment decreases when the fibers are spun into water ($f = 0.38$) compared to those prepared in dilute acetone ($f = 0.44$), and consequently, the Young's modulus and tensile strength decrease by 11.32% and 8.81%, respectively, while the toughness increases by 20.73%. However, analyzing the results from the fibers spun

into a HCl solution, although they show the lowest degree of ANFs alignment ($f = 0.37$), stiffness, and strength among the three conditions, they fail to show the highest toughness with the reduced stiffness. This result implies that the spinning with a rapid protonation rate creates excessively disordered ANFs, which means that the intermolecular contact for hydrogen bonding is not enough to form an entirely stable structure and the disorder cause defect that leads to short elongation. Furthermore, it is demonstrated that ANF assembly with a certain degree of disorder with less defect can induce high toughness rather than having higher alignments with a crystallization tendency (Figure S6, Supporting Information). As another example of the crystallization tendency, the addition of an annealing step based on the fibers prepared in dilute acetone shows decreased toughness by 48.52% while improving modulus by 23.52%.

This result motivates further study to improve the toughness by reducing the degree of alignment of ANFs based on the experimental condition with the 0.2 wt.% ANFs colloidal suspension and dilute acetone, which produced high strength and stiffness fibers with the highest degree of ANFs alignment. To induce mild disorder of ANFs in the spun fiber, a smaller diameter dispensing needle with an inner diameter of 100 μm was introduced. The small diameter needle reduces the ANFs orientation since the die swelling effect becomes prominent, and the drawing ratio is reduced to account for the reduced diameter of the gel-state fibers. These modifications yield fibers with the highest toughness values in this study of $128.66 \pm 14.13 \text{ MJ m}^{-3}$, an increase of >70% compared to the control group, while the modulus and strength only decreased by 11.27% and 6.99%, respectively (Figure 3c,d,f). This approach successfully improves toughness while maintaining much of the strength and stiffness, and it is confirmed that the reduced diameter of the spun fiber with the mild disorder is able to form more optimal entanglement conditions in the nanofiber networks leading to a tougher structure.

A comparative analysis was performed on the mechanical properties of commercial aramid fibers as precursors and prepared ANF-assembled fibers with various experimental conditions (Figure 3g). The commercial aramid fiber (Kevlar KM2+) properties were taken with a Young's modulus of 84.62 GPa, a tensile strength of 3.88 GPa, and a toughness of 80.25 MJ/m³ from previous studies.^[16,31] When the properties of aramid fibers are set to 100% in the radar chart of Figure 3g with three different mechanical properties, the toughness of the fiber obtained from dilute acetone as a control group displays 94.31% of the precursor's properties, while the modulus and strength are 50.85% and 34.89%, respectively. Moreover, the toughness of the fibers prepared in dilute acetone with the narrow outlet corresponding to the highest value is equivalent to 160.32% of the aramid fibers, and the Young's modulus of the fiber produced through the additional annealing process shows the highest value in this study corresponds to 62.81% of the precursor. In terms of tensile strength, unlike other properties that have changed significantly depending on the experimental conditions, its value only ranges from 31% to 35%, indicating signs of convergence.

The ANF-assembled fibers, made by simultaneous protonation and wet spinning, have 60% greater toughness than commercial Kevlar fibers while also having 4.86% lower density, resulting in a vastly improved specific toughness. Given the importance of weight in fiber-reinforced polymer composites, the results of this study show that the ANF spun fibers could be used to create composite materials with high specific energy to break. The specific properties of various fibers are plotted in Figure 4a,b and demonstrate the superior energy to break of the ANF-assembled fibers comparing the specific modulus and strength with other macroscale synthetic and natural fibers except for composite materials (Figure 4). According to the chart, the conventional synthetic fibers are distributed in specific strength and modulus over a broad spectrum while not

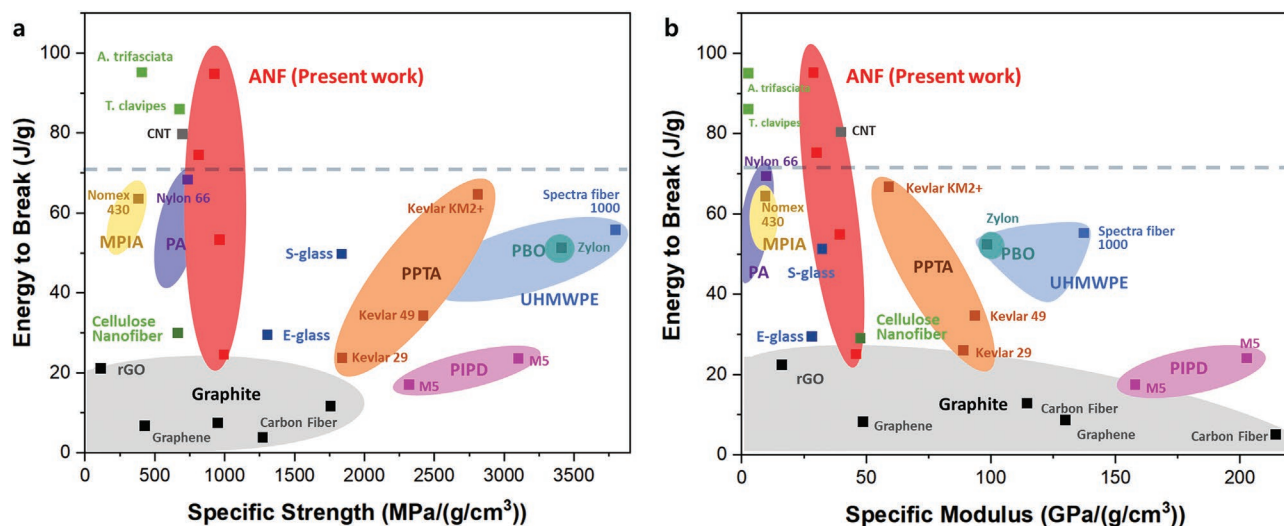


Figure 4. Material mechanical property charts of synthetic fibers and natural fibers. a) Energy to break versus specific strength. b) Energy to break versus specific modulus. The materials include the ANF-assembled fibers prepared in this work shown in the red zone, natural fibers (natural silk, cellulose nanofiber assembly),^[9,21,32,33] polyamide (PA),^[34] poly(meta-phenylene isophthalamide) (MPIA),^[35] poly(p-phenylene terephthalamide) (PPTA),^[16,31] poly(p-phenylenebenzobisthiazole) (PBO),^[36] Ultra-high-molecular-weight polyethylene (UHMWPE),^[37] poly(diimidazopyridinylene dihydroxyphenylene) (PIPD),^[22] carbon nanotube assembly (CNT),^[23] glass fibers^[34,36] and graphite-based fibers.^[38–40]

exceeding the level of $\approx 70 \text{ J g}^{-1}$ in terms of energy to break. As an exceptional case, the multilayered carbon nanotube yarns manufactured by a chemical vapor deposition spinning process have been reported with energy to break of $\approx 80 \text{ J g}^{-1}$.^[23] In the present work, ANF-assembled fibers in the form of monofilament have shown the energy to break over 93 J g^{-1} , and this result demonstrates that it has impressive toughness exceeding other existing macroscale synthetic and natural fibers made of a single component. Furthermore, comparing the present work to spider silks, although the energy to break of the silk drawn from an adult *Nephila edulis* female under specific spinning conditions has been reported to be $\approx 165 \text{ J g}^{-1}$, the results from this work have similar or higher toughness to the silk from *Argiope trifasciata* and *Trichonephila clavipes*.^[21,32,33] Moreover, the ANF-assembled fibers exhibit a specific strength in the range from 945.80 to 1016.29 MPa $\text{g}^{-1} \text{ cm}^3$ and a specific modulus from 28.50 to 39.90 GPa $\text{g}^{-1} \text{ cm}^3$, which are higher than polyamide (PA), poly(meta-phenylene isophthalamide) (MPIA), and natural fibers such as spider silk and nanocellulose fiber. In particular, the strong modulus with high toughness is advantageous for stable energy absorption in the early stage of impact. Therefore, the fibers prepared in this work demonstrate their unique potential for use as a structural reinforcement with properties unlike other fiber technologies.

Recently, the problem of environmental pollution has become a significant issue regarding discarded synthetic fibers after damage. To cope with the issue of waste plastics, a recycling experiment was conducted to refabricate the fibers by dissolving the spun ANF fibers into a DMSO/water/KOH system through a second deprotonation process (Figure S1, Supporting Information) and then repeating the spinning process. The recycled fibers have a Young's modulus of $38.25 \pm 2.91 \text{ GPa}$, showing no difference from a previous experimental case of ANF-acetone (narrow) (Figure 3c,d). However, the tensile strength and toughness decreased by $\approx 6\%$ and 12% , respectively, to $1182.70 \pm 71.96 \text{ MPa}$ and $113.19 \pm 12.83 \text{ MJ m}^{-3}$ (Figure 3d,f). Although this result is considered a chemical degradation due to repeated deprotonation during the recycling process, the recycled fibers still display high mechanical properties, indicating a viable process to yield a sustainable and recyclable material.

3. Conclusion

These results suggest the potential of ANF-assembled fibers as new sustainable functional synthetic fibers by successfully assembling the nanofibers into a macroscale structure with lightweight and outstanding mechanical properties. The ANFs assembly was established by designing a simultaneous protonation and wet spinning process with disorder control, thereby fabricating the ANF-assembled fibers with remarkable toughness that exceeds existing commercial synthetic and natural fibers. Furthermore, it was found that although the prepared fibers formed by the same intermolecular bonding mechanism and coterminous chemical structure as commercial aramid fibers, a unique ANFs network leads to notable mechanical properties. To date, various structural applications based on ANFs have been to capitalize upon the remarkable properties

of aramid fibers. Nevertheless, no breakthrough research has been conducted on the high mechanical properties of a structure composed of ANFs. The results of this study demonstrate the assembly of ANFs with high specific toughness, strength and modulus, thermal stability, and sustainability to be used in structural applications in a broad area, including transportation, aerospace, ballistics, and medical devices. Furthermore, the process developed here requires low energy consumption and is a low-cost, simple, and scalable procedure for the continuous manufacture of fibers with extraordinary toughness.

4. Experimental Section

Materials and Chemicals: KM2+ aramid fabric (Kevlar KM2+, style 790, CS-800) was obtained from JPS Composite Materials. Dimethyl sulfoxide (DMSO, ACS certified), potassium hydroxide (KOH, ACS certified), and hydrochloric acid (HCl, ACS certified) were purchased from Fisher Scientific. Acetone (ACS reagent) was purchased from Sigma-Aldrich and Deionized (DI) water was collected from a purification system (PURELAB Ultra, ELGA LabWater).

Preparation of ANFs Colloidal Suspensions: Multiple ANF colloidal suspensions were prepared based on the process reported by Chen et al.^[27] For the solvent systems, 150 mL of DMSO and 6 mL of DI water mixture were prepared. Then, different ratios of the aramid fabric and KOH according to Table S2 (Supporting Information) with various concentrations (denoted as 0.2, 0.5, 1.0, and 1.5 wt.%) were stirred in the prepared solvent for 3 days at room temperature.

Fabrication of ANF-Assembled Fibers: The first step in fabricating the ANF-assembled fibers is producing gel-state fibers through wet spinning. The wet spinning process consists of three steps: coagulation, washing, and stretching. At the coagulation step, the colloidal suspensions with varying concentrations of ANFs were loaded into 10 mL syringes and extruded by a high precision fluid dispenser (Ultimus V, Nordson EFD) with a 72 cm min^{-1} spinning speed through a flat end stainless-steel needle with an inner diameter of $150 \mu\text{m}$ and a length of 50 mm into three different coagulant baths at ambient temperature. The three different coagulation agents were selected to vary protonation rates and were prepared with 30 wt.% acetone, DI water, and a 0.05 M HCl aqueous solution. Gel-state fibers were spun into the coagulation bath and allowed to sit in the bath for 15 min. The gel-state fibers were then dredged from the coagulation bath, then twice immersed in clean DI water baths. The protonated fibers were then cut into 10 cm long sections that were then stretched using a manual translation stage to 120%. Finally, the fibers were collected, hung on a drying rack, and dried in a vacuum oven at $140 \text{ }^\circ\text{C}$ for 24 h to remove residual solvent. For an additional annealing process, the vacuum-dried fibers were placed in a 125 mL stainless-steel autoclave reactor (Model 4748, Parr Instrument Company) and heated in a convection oven (Heratherm OMH60, Thermo Scientific) to $300 \text{ }^\circ\text{C}$ at $5 \text{ }^\circ\text{C min}^{-1}$ before holding for 5 h.

Morphological and Chemical Characteristics: The isolated ANFs were redispersed in DI water after vacuum filtration with acetone and DI water for washing and drop cast on the oxygen plasma-treated silicon wafer. The isolated ANFs were inspected by atomic force microscopy (AFM, XE-70, Park Systems). The cross-section area, surface, and knot of fabricated ANF-assembled fibers were characterized and imaged through a scanning electron microscope (SEM, JSM-7800FLV, JEOL). The elements in the prepared fibers were analyzed by energy-dispersive X-ray spectroscopy (EDS) equipped with the SEM.

The chemical composition of the commercial aramid fiber and the ANF-assembled fibers were studied using Fourier transform infrared spectroscopy (FTIR, Nicolet is50 spectrometer, Thermo Scientific) with a SMART iTR accessory ranging from 650 to 4000 cm^{-1} at a resolution of 0.4 cm^{-1} . The crystal structures of the prepared fibers were analyzed by using an X-ray diffractometer (XRD, Ultima IV, Rigaku) with a Cu $K\alpha$ radiation source ($\lambda = 0.154 \text{ nm}$). The crystallinity was calculated by the formula defined as

$$\text{Crystallinity} = \frac{A_{002} + A_{110} + A_{200} + A_{004}}{A_{002} + A_{110} + A_{200} + A_{004} + A_{\text{am}}} \quad (1)$$

where A_{hkl} and A_{am} are the peak areas according to lattice planes and amorphous regions. The peak was fit using data analysis software (OriginLab), assuming Gaussian functions of the (002), (110), (200), (004), and amorphous peaks.

Moreover, azimuthal angle scanning was conducted using the same instrument at the $2\theta = 22.8^\circ$, corresponding to the (200) crystal planes, to estimate crystalline alignment in the fabricated fibers. The alignment of ANFs was quantified by Herman's orientation function (f), which is defined as

$$f = \frac{3}{2} \cos^2 \varnothing - \frac{1}{2} \quad (2)$$

$$\cos^2 \varnothing = \frac{\int_0^{\pi/2} I(\varnothing) \cos^2(\varnothing) \sin(\varnothing) d\varnothing}{\int_0^{\pi/2} I(\varnothing) \sin(\varnothing) d\varnothing} \quad (3)$$

where \varnothing as the azimuth angle is the angle (in radians) of the chain axis relative to the interested reference axis. $I(\varnothing)$ is the intensity along the azimuth angle at $2\theta = 22.8^\circ$. Within the orientation in the interest direction, f has a value between 0 and 1 means a higher degree of alignment to the reference axis.

The thermal stability of the aramid fiber and ANF-assembled fibers was studied using a thermogravimetric analyzer (TGA, SDT Q600, TA Instruments) performed at the rate of $10^\circ\text{C min}^{-1}$. The decomposition temperature was confirmed through derivative thermogravimetric analysis (DTG, 1st derivative of the TGA curve).

Mechanical Characterization: Tensile testing was performed according to ASTM D3379 to evaluate a Young's modulus, tensile strength, strain at break, and toughness of the ANF-assembled fibers. As described in ASTM D3379, the fibers were attached to a sample holder made of heavy-weight paper with epoxy such that a gauge length of 12.7 mm was obtained. The tests were carried out at a crosshead speed of 1.92 mm min^{-1} on a universal load frame (5982 series with a 5 N load cell, Instron), and ten specimens were tested for each condition.

Recycled ANF-Assembled Fibers: The recyclability of the ANF-assembled fiber was characterized by 0.3 g of ANF-assembled fibers prepared using a dilute acetone solution with a 0.2 wt.% ANF colloidal suspension. The fibers were mechanically stirred with 150 mL of DMSO, 6 mL of DI water, and 0.45 g of KOH for 7 days to obtain a recycled ANFs colloidal suspension. Then, recycled ANF-assembled fibers were manufactured using the same method described above, and the mechanical properties were evaluated.

Supporting Information

Supporting Information is available from the Wiley Online Library or from the author.

Acknowledgements

This research was supported by the National Research Foundation of Korea (NRF) (NRF-2021R1A6A3A03043273), the Air Force Office of Scientific Research through Contract number FA9550-21-1-0019, and Army Research Office Contract number W911NF-18-1-0061.

Conflict of Interest

The authors declare no conflict of interest.

Data Availability Statement

The data that support the findings of this study are available from the corresponding author upon reasonable request.

Keywords

aramid nanofibers, mechanical properties, protonation, toughness, wet spinning

Received: July 27, 2022

Revised: October 6, 2022

Published online: November 22, 2022

- [1] S. Nagane, S. Macpherson, M. A. Hope, D. J. Kubicki, W. Li, S. D. Verma, J. Ferrer Orri, Y.-H. Chiang, J. L. MacManus-Driscoll, C. P. Grey, S. D. Stranks, *Adv. Mater.* **2021**, *33*, 2102462.
- [2] K. R. Paton, E. Varrla, C. Backes, R. J. Smith, U. Khan, A. O'Neill, C. Boland, M. Lotya, O. M. Istrate, P. King, T. Higgins, S. Barwich, P. May, P. Puczkarski, I. Ahmed, M. Moebius, H. Pettersson, E. Long, J. Coelho, S. E. O'Brien, E. K. McGuire, B. M. Sanchez, G. S. Duesberg, N. McEvoy, T. J. Pennycook, C. Downing, A. Crossley, V. Nicolosi, J. N. Coleman, *Nat. Mater.* **2014**, *13*, 624.
- [3] M. Zhong, R. Wang, K. Kawamoto, B. D. Olsen, J. A. Johnson, *Science* **2016**, *353*, 1264.
- [4] M. Eder, S. Amini, P. Fratzl, *Science* **2018**, *362*, 543.
- [5] M. R. Begley, D. S. Gianola, T. R. Ray, *Science* **2019**, *364*, eaav4299.
- [6] S. C. Glotzer, M. J. Solomon, *Nat. Mater.* **2007**, *6*, 557.
- [7] K. Thorkelsson, P. Bai, T. Xu, *Nano Today* **2015**, *10*, 48.
- [8] H. C. Kim, J. W. Kim, L. Zhai, J. Kim, *Cellulose* **2019**, *26*, 5821.
- [9] N. Mittal, F. Ansari, K. GowdaV, C. Brouzet, P. Chen, P. T. Larsson, S. V. Roth, F. Lundell, L. Wågberg, N. A. Kotov, L. D. Söderberg, *ACS Nano* **2018**, *12*, 6378.
- [10] A. T. L. Tan, J. Beroz, M. Kolle, A. J. Hart, *Adv. Mater.* **2018**, *30*, 1803620.
- [11] D. Puppi, F. Chiellini, *Polym. Int.* **2017**, *66*, 1690.
- [12] H. C. Kim, P. S. Panicker, D. Kim, S. Adil, J. Kim, *Sci. Rep.* **2021**, *11*, 13611.
- [13] M. Yang, K. Cao, L. Sui, Y. Qi, J. Zhu, A. Waas, E. M. Arruda, J. Kieffer, M. D. Thouless, N. A. Kotov, *ACS Nano* **2011**, *5*, 6945.
- [14] J. Nasser, L. Zhang, J. Lin, H. Sodano, *ACS Appl Polym Mater* **2020**, *2*, 2934.
- [15] J. Lin, S. H. Bang, M. H. Malakooti, H. A. Sodano, *ACS Appl. Mater. Interfaces* **2017**, *9*, 11167.
- [16] J. Nasser, J. Lin, K. Steinke, H. A. Sodano, *Compos. Sci. Technol.* **2019**, *174*, 125.
- [17] Y. Zhao, X. Li, J. Shen, C. Gao, B. Van der Bruggen, *J. Mater. Chem. A* **2020**, *8*, 7548.
- [18] B. Yang, L. Wang, M. Zhang, J. Luo, Z. Lu, X. Ding, *Adv. Funct. Mater.* **2020**, *30*, 2000186.
- [19] A. Wang, X. Zhang, F. Chen, Q. Fu, *Carbon* **2021**, *179*, 655.
- [20] Z. Liu, J. Lyu, D. Fang, X. Zhang, *ACS Nano* **2019**, *13*, 5703.
- [21] F. Vollrath, D. P. Knight, *Nature* **2001**, *410*, 541.
- [22] P. M. Cuniff, M. A. Auerbach, presented at *23rd. Army Science Conf.*, Orlando, **2002**.
- [23] X.-H. Zhong, Y.-L. Li, Y.-K. Liu, X.-H. Qiao, Y. Feng, J. Liang, J. Jin, L. Zhu, F. Hou, J.-Y. Li, *Adv. Mater.* **2010**, *22*, 692.
- [24] H. C. Kim, D. Kim, J. Y. Lee, L. Zhai, J. Kim, *Int. J. Precis. Eng. Manuf.-Green Technol.* **2019**, *6*, 567.
- [25] S. Seyedin, M. S. Romano, A. I. Minett, J. M. Razal, *Sci. Rep.* **2015**, *5*, 14946.

- [26] S. Suto, S. Yoshida, *Angew. Makromol. Chem.* **1995**, 226, 89.
- [27] H.-J. Chen, Q.-Y. Bai, M.-C. Liu, G. Wu, Y.-Z. Wang, *Green Chem.* **2021**, 23, 7646.
- [28] M. Zhang, K. R. Atkinson, R. H. Baughman, *Science* **2004**, 306, 1358.
- [29] X. Liao, M. Dulle, J. M. de Souza e Silva, R. B. Wehrspohn, S. Agarwal, S. Förster, H. Hou, P. Smith, A. Greiner, *Science* **2019**, 366, 1376.
- [30] N. P. Cheremisinoff, P. N. Cheremisinoff, *Handbook of Applied Polymer Processing Technology*, CRC Press, Boca Raton, FL **2020**.
- [31] M. Cheng, W. Chen, T. Weerasooriya, *J Eng Mater Technol* **2005**, 127, 197.
- [32] B. O. Swanson, T. A. Blackledge, A. P. Summers, C. Y. Hayashi, *Evolution* **2006**, 60, 2539.
- [33] T. A. Blackledge, C. Y. Hayashi, *J Exp Biol* **2006**, 209, 2452.
- [34] J. B. Gillespie, D. D. Edie, V. Gabara, T. J. Haulik, J. L. Kardos, L. S. Schadler, *High-Performance Structural Fibers for Advanced Polymer Matrix Composites*, National Academies Press, Washington, DC, **2005**, p. 11268.
- [35] R. Zaera, in *Impact Engineering of Composite Structures* (Ed: S. Abrate), Springer, Vienna, **2011**, p. 305.
- [36] M. N. Mohammed, S. Al-Zubaidi, S. H. K. Bahrain, S. M. Sapuan, in *Composite Solutions for Ballistics*, Elsevier, Cham **2021**, p. 3.
- [37] A. Bhatnagar, *Lightweight Ballistic Composites*, CRC Press, Boca Raton, FL **2006**.
- [38] Z. Xu, Y. Liu, X. Zhao, L. Peng, H. Sun, Y. Xu, X. Ren, C. Jin, P. Xu, M. Wang, C. Gao, *Adv. Mater.* **2016**, 28, 6449.
- [39] X. Xiang, Z. Yang, J. Di, W. Zhang, R. Li, L. Kang, Y. Zhang, H. Zhang, Q. Li, *Nanoscale* **2017**, 9, 11523.
- [40] G. Xin, T. Yao, H. Sun, S. M. Scott, D. Shao, G. Wang, J. Lian, *Science* **2015**, 349, 1083.